

A next-to-leading order QCD analysis of deeply virtual Compton scattering amplitudes

Andreas Freund*

Institut für Theoretische Physik, University of Regensburg, Universitätstr. 31, 93053 Regensburg, Germany

Martin McDermott†

Division of Theoretical Physics, Dept. Math. Sciences, University of Liverpool, Liverpool, L69 3BX, UK

(May 20, 2019)

We present a next-to-leading order (NLO) QCD analysis of unpolarized and polarized deeply virtual Compton scattering (DVCS) amplitudes, for two different input scenarios, in the \overline{MS} scheme. We illustrate and discuss the size of the NLO effects and the behavior of the amplitudes in skewedness, ζ , and photon virtuality, Q^2 . In the unpolarized case, at fixed Q^2 , we find a remarkable power-law behaviour in ζ , akin to Regge factorization, over several orders of magnitude in ζ . We also quantify the ratio of real to imaginary parts of the DVCS amplitudes and their sensitivity to changes of the factorization scale.

I. INTRODUCTION

Deeply virtual Compton scattering (DVCS) [1–8], $\gamma^*(q) + p(P) \rightarrow \gamma(q') + p(P')$, is the most promising process for accessing generalized parton distributions (GPDs) [1–3,9–11] which carry new information about the dynamical degrees of freedom inside a nucleon. GPDs are an extension of the well-known parton distribution functions (PDFs) appearing in inclusive processes and are defined as the Fourier transform of *non-local* light-cone operators sandwiched between nucleon states of *different* momenta, commensurate with a finite momentum transfer in the t-channel. These distributions are true two-particle correlation functions and contain, in addition to the usual PDF-type information residing in the DGLAP [12] region, supplementary information about the distribution amplitudes of virtual meson-like states in the nucleon in the ERBL [13] region. We recently presented a full numerical solution of the associated renormalization group equations at next-to-leading order (NLO) accuracy, for unpolarized and polarized distributions, using realistic input models [14], as well as a complete NLO QCD analysis of DVCS observables [15]. To achieve this we calculated the real and imaginary parts of unpolarized and polarized DVCS amplitudes, $\mathcal{T}_{DVCS}^{V/A}$, at NLO which is related to the triple differential cross

section on the lepton level via

$$\begin{aligned} \frac{d\sigma^{(3)}(e^\pm p \rightarrow e^\pm \gamma p)}{dx_{bj}dQ^2d|t|} &= \int_0^{2\pi} d\phi \frac{d\sigma^{(4)}}{dx_{bj}dQ^2d|t|d\phi} \\ &= \frac{\alpha_{e.m.}^3 x_{bj} y^2}{8\pi Q^4} \left(1 + \frac{4M^2 x_{bj}^2}{Q^2}\right)^{-1/2} \int_0^{2\pi} d\phi |\mathcal{T}^\pm|^2, \end{aligned} \quad (1)$$

where

$$|\mathcal{T}^\pm|^2 = |\mathcal{T}_{DVCS}|^2 \pm (\mathcal{T}_{DVCS}^* \mathcal{T}_{BH} + \mathcal{T}_{DVCS} \mathcal{T}_{BH}^*) + |\mathcal{T}_{BH}|^2.$$

The dependent variables Q^2, x_{bj}, t are the photon virtuality, Bjorken x and the momentum transfer to the proton squared, respectively, ϕ is the relative angle between the lepton and proton scattering planes [16], $y = Q^2/x_{bj}S$ is the energy fraction of the incoming lepton carried by the photon, S is the total center of mass energy and M is the proton mass.

The real and imaginary parts of the polarized and unpolarized DVCS amplitudes are interesting in their own right, since each can be independently accessed experimentally via various asymmetries which exploit the ϕ -dependence of the interference term [7,17]. Thus the predictions that we give here for the real and imaginary parts of the amplitudes at NLO, their behavior in the skewedness, ζ , and Q^2 , as well as the relationship between real and imaginary parts, which all depend on the GPDs, can be directly tested by experiment. A NLO analysis of the DVCS amplitudes for large ζ was carried out in [18] and, at the limited points where a comparison is possible, we agree with their results.

This paper is structured as follows. In Section II we define the input model for the GPDs and briefly review their NLO evolution. We state the necessary factorized convolution integrals and explain their exact technical implementation, via subtractions. In Section III we give detailed NLO results for the real and imaginary parts of the unpolarized (subsection III A) and polarized (subsection III B) DVCS amplitudes, comparing them to LO results using the same input GPDs and commenting on their sensitivity to the input GPDs and the factorization scale, μ^2 . We also give the Q^2 and ζ dependence of the ratio of real to imaginary parts and quantize the importance of the ERBL region to the real part. We close our discussion in Section IV with a statement on the general structure of NLO and NNLO corrections and briefly

*andreas.freund@physik.uni-regensburg.de

†martinmc@amtp.liv.ac.uk

conclude in Section V. For convenience in an appendix (section VI) we restate the NLO coefficient functions [18] (in VIA) and give analytic results for their integrals (in VIB), which are required to implement the subtractions in section III.

II. FACTORIZATION THEOREM AND DEFINITIONS

There are many representations for GPDs [1–3,9–11,19], we chose to work in a particular representation identical to the non-diagonal representation defined in [19] which is a natural one when comparing to experiments. We use

$$\begin{aligned} \mathcal{F}^{S(a),V/A}(X, \zeta, \mu^2, t) &= \\ &\left[\frac{H^{a,V/A}(v, \zeta, \mu^2, t) \mp H^{a,V/A}(-v, \zeta, \mu^2, t)}{(1 - \zeta/2)} \right], \\ \mathcal{F}^{g,V/A}(X, \zeta, \mu^2, t) &= \\ &\left[\frac{H^{g,V/A}(v, \zeta, \mu^2, t) \pm H^{g,V/A}(-v, \zeta, \mu^2, t)}{(1 - \zeta/2)} \right], \end{aligned} \quad (2)$$

where $v = (X - \zeta/2)/(1 - \zeta/2)$, $S(a)$ and g refers to the quark singlet for flavour a and gluon, respectively, V and A stand for unpolarized (vector) and polarized (axial-vector) cases, taking the upper and lower signs, respectively. This representation is different from the usual one (see for example [9]) which is defined symmetrically with respect to the incoming and outgoing nucleon plus momentum (defined on the interval $v \in [-1, 1]$ and symmetric about $v = 0$). The GPDs in eq. (2) have plus momentum fractions (on the interval $X \in [0, 1]$) with respect to the incoming nucleon momentum, P , in analogy to the PDFs of inclusive reactions, with the ERBL region in the interval $X \in [0, \zeta]$ and the DGLAP region in the interval $X \in [\zeta, 1]$. The transformation between the symmetric and non-diagonal representation is given in [19]. Furthermore, within the non-diagonal representation $\zeta = x_{bj} = -q^2/2P \cdot q$ and the symmetry of the GPDs, which was previously manifest about $v = 0$, is now manifest about the point $X = \zeta/2$.

We build input distributions, $\mathcal{F}^{S(a),g}(X, \zeta, Q_0)$, at the input scale, Q_0 , with the correct symmetries and properties, from conventional PDFs in the DGLAP region, for both the unpolarized and polarized cases, by employing the factorized model due to Radyushkin [20], which is based on double distributions. The H functions (symmetric GPDs) required for eq.(2) are related to the latter via the following reduction formula (factoring out the overall t -dependence):

$$H(v, \zeta) = \int_{-1}^1 dx' \int_{-1+|x'|}^{1-|x'|} dy' \delta\left(x' + \frac{\zeta y'}{2 - \zeta} - v\right) F(x', y'). \quad (3)$$

The double distributions, $F^{i,V/A}$, are a product of a profile function, π^i , and a conventional PDF, $f^{i,V/A}$, ($i = q(a), g$):

$$\begin{aligned} F^{q(a)}(x', y') &= \pi^q(x', y') f^{q(a)}(x') \\ &= \frac{3}{4} \frac{(1 - |x'|)^2 - y'^2}{(1 - |x'|)^3} f^{q,a}(x'), \\ F^g(x', y') &= \pi^g(x', y') f^g(x') \\ &= \frac{15}{16} \frac{((1 - |x'|)^2 - y'^2)^2}{(1 - |x'|)^5} f^g(x'), \end{aligned} \quad (4)$$

where

$$\begin{aligned} f^g(x) &= xg(x, Q_0)\Theta(x) + |x|g(|x|, Q_0)\Theta(-x) \\ f^{q(a)}(x) &= q^a(x, Q_0)\Theta(x) - (\bar{q}^a)(x, Q_0)\Theta(-x). \end{aligned} \quad (5)$$

The profile functions are chosen to guarantee the correct symmetry properties in the ERBL region which are preserved under evolution, as we explicitly illustrated in [14]. Their normalization is specified by demanding that the conventional distributions are reproduced in the forward limit at the input scale: $\mathcal{F}^i(X, \zeta \rightarrow 0, Q_0) \rightarrow f^i(X, Q_0)$.

In addition to the contributions from the double distributions the unpolarized singlet GPDs also contain a so-called ‘‘D-term’’ [21,22], which is only non-zero in the ERBL region, and ensures the correct polynomiality in ζ [22] of the GPDs moments in X . There is an equivalent term in the unpolarized gluon distribution but apart from its symmetry nothing is known about this function, thus we chose to set it to zero.

Within the above class of input model, we specify two particular input models for the GPDs by using two sets of inclusive unpolarized/polarized PDFs (for use in eqs.(2,3,4)), i.e. GRV98/GRSV00 [23] with $\Lambda_{\text{QCD}}^{(4,NLO)} = 246$ MeV and MRSA'/GS(A) [24] with $\Lambda_{\text{QCD}}^{(4,NLO)} = 231$ MeV at the common input scale $Q_0^2 = 4$ GeV² and $\Lambda_{\text{QCD}}^{(4,LO)} = 174$ MeV for both sets. Using two different choices allows us to investigate the sensitivity of the amplitudes to the choice of input. The GPDs are then evolved in LO and NLO using our newly developed evolution code [14]. Note that there are two sets of evolution equations which have to be solved simultaneously, one for the ERBL region [13] and one for the DGLAP [12] region, with the ERBL being dependent on the evolution in the DGLAP region, whereas the evolution in the DGLAP region is independent from the evolution in the ERBL region (for more details see [14]).

The factorization theorem [6] proves that the DVCS amplitude takes the following factorized form (in the non-diagonal representation) up to power suppressed contributions in $1/Q$:

$$\mathcal{T}_{DVCS}^{S,V/A}(\zeta, Q^2, t) = \sum_a e_a^2 \left(\frac{2 - \zeta}{\zeta}\right) [P.V.]$$

$$\begin{aligned}
& \int_0^1 dX T^{S(a),V/A} \left(\frac{2X}{\zeta} - 1, \frac{Q^2}{\mu^2} \right) \mathcal{F}^{S(a),V/A}(X, \zeta, \mu^2, t) \mp \\
& \int_{\zeta}^1 dX T^{S(a),V/A} \left(1 - \frac{2X}{\zeta}, \frac{Q^2}{\mu^2} \right) \mathcal{F}^{S(a),V/A}(X, \zeta, \mu^2, t) \Big], \\
\mathcal{T}_{DVCS}^{g,V/A}(\zeta, \mu^2, t) &= \frac{1}{N_f} \left(\frac{2-\zeta}{\zeta} \right)^2 \left[P.V. \right. \\
& \int_0^1 dX T^{g,V/A} \left(\frac{2X}{\zeta} - 1, \frac{Q^2}{\mu^2} \right) \mathcal{F}^{g,V/A}(X, \zeta, \mu^2, t) \pm \\
& \left. \int_{\zeta}^1 dX T^{g,V/A} \left(1 - \frac{2X}{\zeta}, \frac{Q^2}{\mu^2} \right) \mathcal{F}^{g,V/A}(X, \zeta, \mu^2, t) \right]. \tag{6}
\end{aligned}$$

In the following we will initially set the factorization scale, μ^2 , equal to the photon virtuality, Q^2 , and will later investigate its variation. The LO and NLO coefficient functions, $T^{i,V/A}$, are taken from eqs.(14-17) of [18] and are summarized in the appendix VIA. They can have both real and imaginary parts, depending on the region of integration, which in turn generates real and imaginary parts of the DVCS amplitudes. Henceforth, we will suppress the factorized t -dependence since all of our predictions will be made for $t = 0$. *P.V.* stands for the Cauchy principal value prescription which needs to be applied only to the $0 - 1$ integral. We chose to implement it through the following algorithm:

$$\begin{aligned}
P.V. \int_0^1 dX T \left(\frac{2X}{\zeta} - 1 \right) \mathcal{F}(X, \zeta, Q^2) &= \\
& \int_0^{\zeta} dX T \left(\frac{2X}{\zeta} - 1 \right) (\mathcal{F}(X, \zeta, Q^2) - \mathcal{F}(\zeta, \zeta, Q^2)) + \\
& \int_{\zeta}^1 dX T \left(\frac{2X}{\zeta} - 1 \right) (\mathcal{F}(X, \zeta, Q^2) - \mathcal{F}(\zeta, \zeta, Q^2)) + \\
& \mathcal{F}(\zeta, \zeta, Q^2) \int_0^1 dX T \left(\frac{2X}{\zeta} - 1 \right), \tag{7}
\end{aligned}$$

each term in eq. (7) is now either separately finite or only contains an integrable logarithmic singularity. This algorithm closely resembles the implementation of the $+$ regularization in the evolution of PDFs and GPDs. Note that the first integral in eq. (7) (in the ERBL region) is strictly real, however, the second and third terms contain both real and imaginary parts (which are generated in the DGLAP region). This definition leads to the following formulas for the real and imaginary parts of the DVCS amplitudes:

$$\begin{aligned}
\text{Re } \mathcal{T}_{DVCS}^{S,V/A}(\zeta, Q^2) &= \sum_a e_a^2 \left(\frac{2-\zeta}{\zeta} \right) \left[\right. \\
& \left. \int_0^{\zeta} dX T^{S,V/A}(z) \left(\mathcal{F}^{S,V/A}(X, \zeta) - \mathcal{F}^{S,V/A}(\zeta, \zeta) \right) + \right.
\end{aligned}$$

$$\begin{aligned}
& \int_{\zeta}^1 dX \left\{ \text{Re} T^{S,V/A}(z) \left(\mathcal{F}^{S,V/A}(X, \zeta) - \mathcal{F}^{S,V/A}(\zeta, \zeta) \right) \right. \\
& \left. \mp \text{Re} T^{S,V/A}(-z) \mathcal{F}^{S,V/A}(X, \zeta) \right\} \\
& + \mathcal{F}^{a,V/A}(\zeta, \zeta) \text{Re} \int_0^1 dX T^{S,V/A}(z) \Big], \\
\text{Im } \mathcal{T}_{DVCS}^{S,V/A}(\zeta, Q^2) &= \sum_a e_a^2 \left(\frac{2-\zeta}{\zeta} \right) \left[\right. \\
& \int_{\zeta}^1 dX \left\{ \text{Im} T^{S,V/A}(z) \left(\mathcal{F}^{S,V/A}(X, \zeta) - \mathcal{F}^{S,V/A}(\zeta, \zeta) \right) \right. \\
& \left. \mp \text{Im} T^{S,V/A}(-z) \mathcal{F}^{S,V/A}(X, \zeta) \right\} \\
& + \mathcal{F}^{S,V/A}(\zeta, \zeta) \text{Im} \int_0^1 dX T^{S,V/A}(z) \Big], \tag{8}
\end{aligned}$$

$$\begin{aligned}
\text{Re } \mathcal{T}_{DVCS}^{g,V/A}(\zeta, Q^2) &= \frac{1}{N_f} \left(\frac{2-\zeta}{\zeta} \right)^2 \left[\right. \\
& \int_0^{\zeta} dX T^{g,V/A}(z) \left(\mathcal{F}^{g,V/A}(X, \zeta) - \mathcal{F}^{g,V/A}(\zeta, \zeta) \right) + \\
& \int_{\zeta}^1 dX \left\{ \text{Re} T^{g,V/A}(z) \left(\mathcal{F}^{g,V/A}(X, \zeta) - \mathcal{F}^{g,V/A}(\zeta, \zeta) \right) \right. \\
& \left. \pm \text{Re} T^{g,V/A}(-z) \mathcal{F}^{g,V/A}(X, \zeta) \right\} \\
& + \mathcal{F}^{g,V/A}(\zeta, \zeta) \text{Re} \int_0^1 dX T^{g,V/A}(z) \Big], \\
\text{Im } \mathcal{T}_{DVCS}^{g,V/A}(\zeta, Q^2) &= \frac{1}{N_f} \left(\frac{2-\zeta}{\zeta} \right)^2 \left[\right. \\
& \int_{\zeta}^1 dX \left\{ \text{Im} T^{g,V/A}(z) \left(\mathcal{F}^{g,V/A}(X, \zeta) - \mathcal{F}^{g,V/A}(\zeta, \zeta) \right) \right. \\
& \left. \pm \text{Im} T^{g,V/A}(-z) \mathcal{F}^{g,V/A}(X, \zeta) \right\} \\
& + \mathcal{F}^{g,V/A}(\zeta, \zeta) \text{Im} \int_0^1 dX T^{g,V/A}(z) \Big], \tag{9}
\end{aligned}$$

where $z = 2X/\zeta - 1$ and for convenience we have suppressed the scale and explicit quark flavour dependence of the GPDs on the left hand side. The real and imaginary parts of the unpolarized and polarized DVCS amplitudes were computed using a FORTRAN code based on numerical integration routines (for more details see [25]). We implemented the exact solution to the RGE equation for α_s , in LO and NLO as appropriate, in our calculation to be consistent throughout our analysis.

III. NLO AND LO DVCS AMPLITUDES

In the next two subsections we present results for the real and imaginary parts of the NLO DVCS amplitudes

for the unpolarized and polarized cases. We first plot the absolute values, then the ratio of real to imaginary parts (in Q^2 for fixed ζ and in ζ for fixed Q^2). Finally, we discuss the influence of the ERBL region on the real part of the amplitudes and the factorization scale dependence.

A. The unpolarized DVCS amplitudes

In Fig.(1) we plot the real and imaginary parts of the unpolarized quark singlet amplitude (cf. eq. (8)) at LO and NLO.

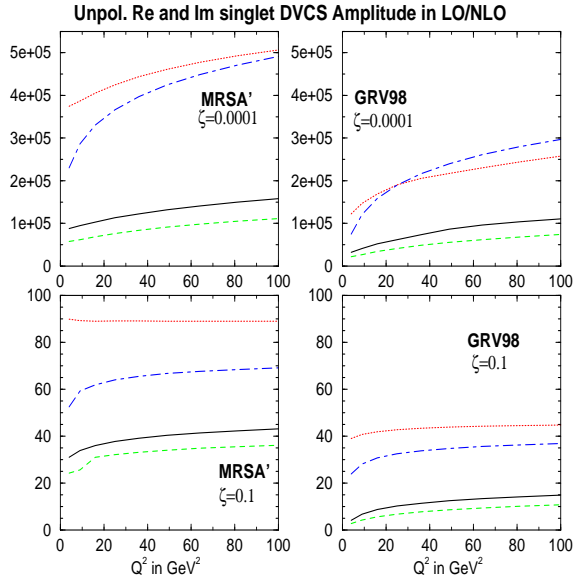


FIG. 1. The Q^2 -dependence of the real and imaginary parts of the quark singlet DVCS amplitude. The solid (dashed) curve is the real part in LO (NLO) and the dotted (dashed-dotted) curve is the imaginary part in LO (NLO).

We observe that the NLO corrections are generally large (between 10% – 100% with the mean between 20 – 50%) and are also strongly input dependent. Some features are the same for both input GPD sets: the NLO corrections tend to decrease the value of the real and imaginary parts of the amplitude. The amplitudes drop dramatically in going from small to large ζ reflecting the strong decrease in the GPDs. They generally increase with increasing Q^2 , albeit moderately, reflecting the expected $\ln(Q^2)$ behavior. In fact, an approximate scaling is observed at LO and NLO, but only sets in at large Q^2 for small ζ in the imaginary part at NLO.

In Fig.(2) we show the real and imaginary parts of the unpolarized gluon amplitude (cf. eq. (9)) which starts at NLO. We note firstly that the gluon contribution is of the same order of magnitude as the quark singlet one, although it is suppressed by $\alpha_s/2\pi$ and secondly that the real part of the gluon amplitude is large and negative. This explains the strong variation of the azimuthal angle asymmetry (AAA), in moving from LO to NLO, observed

in [15] which is directly proportional to the real part of a combination of DVCS amplitudes.

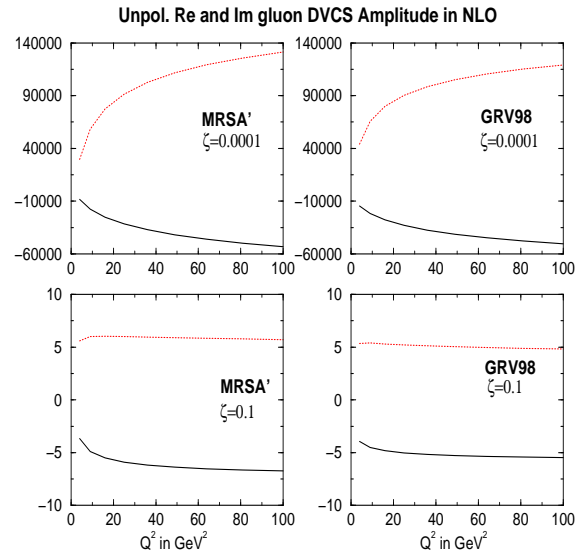


FIG. 2. The Q^2 -dependence of the real (solid line) and imaginary (dotted line) parts of the unpolarized gluon DVCS amplitude, for two representative values of ζ .

Otherwise, the gluon mirrors the NLO quark singlet amplitudes in its behavior in Q^2 and for large and small ζ .

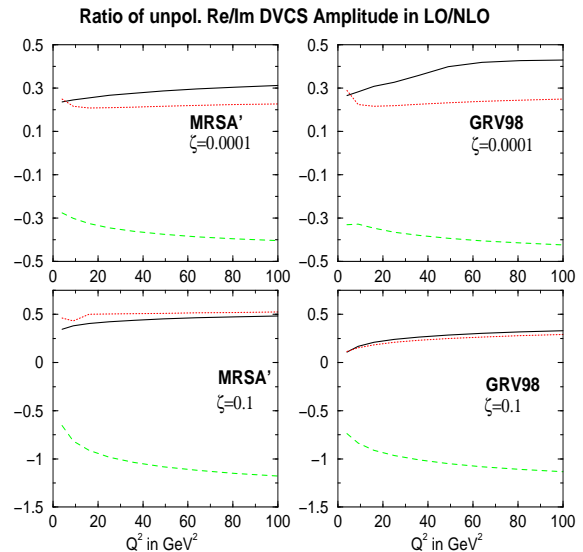


FIG. 3. The ratio of real to imaginary parts of the unpolarized quark singlet and gluon DVCS amplitudes, as a function of Q^2 . The solid (dotted) curve is for the quark singlet in LO (NLO) and the dashed curve is for the gluon in NLO.

In Fig. (3) we show the ratio of the real to imaginary parts for both the quark singlet and the gluon amplitudes as a function of Q^2 . We note that the ratios can be as large as 45% (a similar value was found for the closely related process of J/ψ photoproduction in [26]).

The quark ratios are slightly different for the two inputs. The greatest contrast is seen at small ζ : the NLO case is basically flat in Q^2 which differs markedly from LO which rises with Q^2 . Both cases are similar at large ζ . The gluon ratio is remarkably similar for the two input sets, at both small and large ζ , for the whole Q^2 range considered.

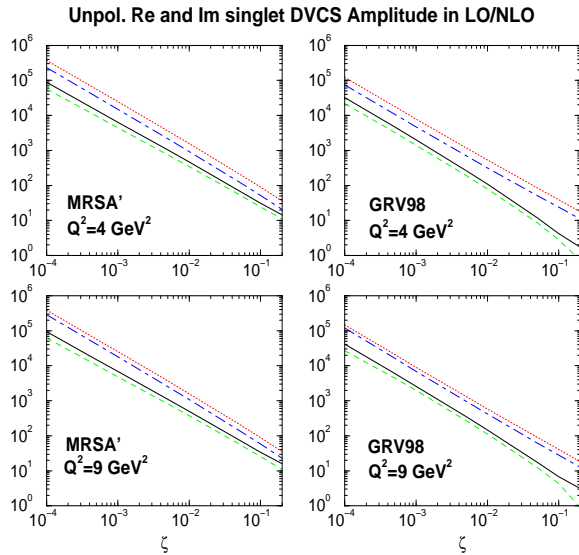


FIG. 4. The real and imaginary parts of the unpolarized quark singlet DVCS amplitude, as a function of ζ . The solid (dashed) curve is the real part in LO (NLO) and the dotted (dashed-dotted) curve is the imaginary part in LO (NLO). A remarkably simple behaviour is observed in ζ which is close to a single power over a wide range. Because Q^2 is fixed, this behaviour in ζ translates directly into a single power in energy.

We now turn to the ζ -dependence for fixed Q^2 which is shown in fig.(4) for the quark singlet and fig.(5) for the gluon. The most striking feature for the quark singlet case is that the amplitudes exhibit a power-like behavior in ζ over basically the *whole* range ($\zeta \in [0.0001, 0.2]$), as illustrated by the straight lines in fig.(4). A simple two parameter fit of the type $a_0\zeta^{\lambda_0}$ works remarkably well up to about $\zeta = 0.1$. The best fit is obtained with a four parameter fit, of the type $c_1\zeta^{\lambda_1}(1 + c_2\zeta^{\lambda_2})$, which can reproduce most of the curves on the few percent level, with λ_0 and λ_1 within 5% – 20% of each other, and λ_2 small. The simple two parameter fit works best for the imaginary part of the amplitudes where we obtain a value for λ_0 between -1.1 and -1.25 with a moderate growth in Q^2 as expected from measurements of the slope of F_2 and HERA diffractive processes. For the real part of the amplitude the simple fit starts to decrease in quality around $\zeta = 0.05$ (depending on the input). The MRSA' input exhibits the power-like behavior over a broader range in ζ , up to about $\zeta = 0.1$.

Similar power-like behaviors have been observed in many small- x processes at HERA, including diffractive

DIS in which the x_P -dependence of diffractive structure functions is known to factorize for small x_P . This behavior, known as Regge factorization, is predicted for high energy processes within Regge theory given the postulate of a universally exchanged Regge pole, known as the Pomeron. Since the relationship between the phenomenological Regge Theory and perturbative QCD remains unresolved, we find the observation of this single power in our perturbative QCD calculation remarkable and very interesting.

The fact that a single power apparently works for such a large range in ζ for DVCS is somewhat surprising. Perhaps this indicates that DVCS always proceeds through partonic configurations which lie in the same universality class, i.e. are self-similar. The reason why these self-similar configuration seem to be of importance beyond the “diffractive region” can be understood if one examines the behavior of the integrand in the convolution integrals in eqs. (8, 9). One observes that the main contribution to the integral and ultimately to the imaginary part of the amplitude itself stems from the region in X very close to ζ , even for larger values of ζ , leading to the self-similar behavior. This is not too surprising given the steep rise of the GPD in the DGLAP region towards ζ and that the coefficient functions are singular at ζ , where even the implementation of the principal value in Sec. (II) leaves an integrable singularity. This situation is somewhat altered for the real part of the amplitude where the ERBL region plays a very important part, as we will see. There, although the coefficient function is singular, the symmetry of the GPD in the ERBL region makes the value of the integral somewhat less dependent on the region near ζ , i.e. less singular, especially for large ζ . Although the value of the real part also depends on an integral over the DGLAP region which contributes more to the power like behavior, this dependence progressively decreases as ζ grows.

The physical picture which is emerging is the following: the region near ζ corresponds to large light-cone distances for the operators which translates into two parton configurations, either a $q\bar{q}$ pair in the ERBL region or a quark leaving and then returning to the proton in the DGLAP region, where one of the partons, either the \bar{q} or the returning q , carries virtually zero momentum fraction, $X - \zeta$, and is thus “soft”, whereas the other carries a momentum fraction of approximately ζ , i.e. a very asymmetric configuration seems to have a disproportionate weighting in the amplitude. The coefficient functions, with their singularity structure at ζ , weight these configurations much more heavily in the amplitude than other, more symmetric, configurations.

Although asymmetric configurations become rare as one approaches the valence region of large ζ , because they should be mainly found in the sea, they are still enhanced by the singularity structure of the coefficient functions. This then leads us to the conclusion that,

although the sea is small at large ζ , DVCS still proceeds largely through sea configurations in the valence region, thus its relative scarcity compared to DIS in the valence region. Physically, at large $X \approx \zeta$, one has to strike an unusual fluctuation in the proton to emit a real photon, while still leaving the proton intact.

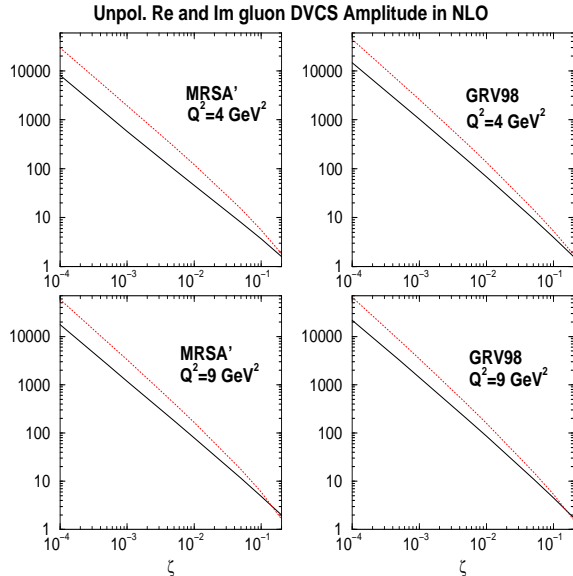


FIG. 5. The real and imaginary parts of the unpolarized gluon DVCS amplitude as functions of ζ , for fixed Q^2 . The solid curve is the real part and the dotted curve is the imaginary part of the gluon amplitude.

As for the gluon we find the same behavior as in the case of the quark singlet. Note that we took the modulus of the real part, since it is actually *negative*, in order to plot both the real and imaginary part on the same log-log plot. Performing the same type of fits as in the quark case, one obtains similar numbers for λ_0 between -1.14 and -1.28 in the two parameter fit and again very similar ones in the four parameter fit (5%–25% variation in the powers). The quality of the two parameter fit starts to decrease rapidly for a $\zeta \sim 0.05$. Nevertheless, the explanation given in the quark singlet case is still applicable in the case of the gluon.

In Fig. (6) we show the ratio of real to imaginary parts in ζ for fixed Q^2 . Again we note the remarkable similarity between the gluon curves for both inputs, both in shape as well as absolute values and the very mild growth behavior for the quark singlet ratio in ζ whereas the gluon varies quite strongly in ζ .

Using Fig. (6) we can make a simple test to check whether we have computed the real part of the amplitude at small ζ properly by employing a dispersion relation for the unpolarized amplitudes at small ζ (for more details see [26]):

$$\frac{|\text{Re } T_{DVCS}|}{\text{Im } T_{DVCS}} = \tan\left(\frac{\pi}{2}(|\lambda| - 1)\right). \quad (10)$$

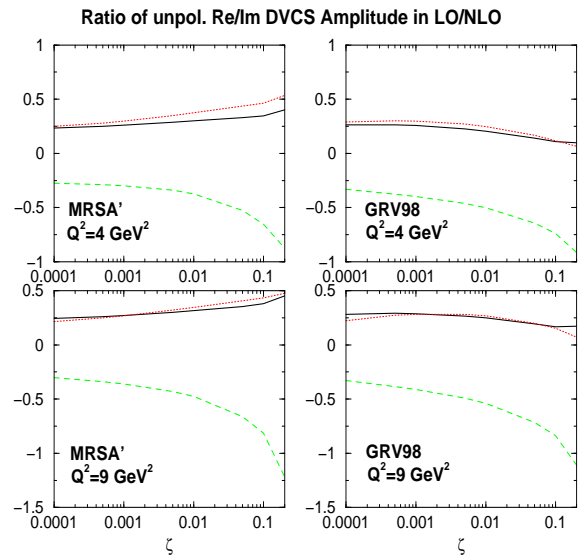


FIG. 6. The ratio of real to imaginary parts of the unpolarized quark singlet and gluon DVCS amplitude, as a function of ζ , at fixed Q^2 . The solid (dotted) curve is the ratio in LO (NLO) and the dashed curve is the ratio for the gluon in NLO.

For the fitted values of λ we obtain a ratio which is in very good agreement with the values in Fig. (6) up to about $\zeta = 5 \times 10^{-3}$ for both the quark singlet and the gluon. This confirms the self-consistency of our calculation.

Next we discuss the relative importance of the ERBL region to the value of the real part of the DVCS amplitude, starting with the quark singlet. On inspection of the relative contribution of the ERBL integrals ($X \in [0, \zeta]$) in eqs. (8, 9) we find that at small ζ the ERBL region integral has a relative contribution between 90% at the input scale and 140% at $Q^2 = 100 \text{ GeV}^2$ (100% and 50% respectively in LO) of the value of the amplitude, i.e. there is a large cancellation between the subtraction term and the $X \in [\zeta, 1]$, integral with both of them being substantially larger, individually than the $[0, \zeta]$ integral. As one increases ζ the relative importance of the ERBL region drops to 50% at the input scale and 130% at $Q^2 = 100 \text{ GeV}^2$ (80% and 30% respectively in LO), however, the subtraction term now starts to dominate the value of the amplitude. This observation is in line with our previous argument of the importance of very asymmetric parton configurations. Remember, that the subtraction term is directly proportional to the GPD at ζ . Also note that going from LO to NLO seems to change the relative importance of the ERBL region, especially its Q^2 behavior. Turning now to the gluon we make a slightly different observation. Firstly, at small ζ the relative contribution varies from 40% – 60% in going from the input scale to $Q^2 = 100 \text{ GeV}^2$ again there is a large cancellation between the previously mentioned terms, but the change in Q^2 is not very dramatic. In-

creasing ζ one finds an increase of the relative importance to 60% – 80% in going from the input scale to our large Q^2 value. Again the subtraction term becomes more and more dominant, relatively speaking, and thus our interpretation from the quark case carries over to the gluon case.

To close our analysis of the unpolarized case, we discuss the scale dependence of the DVCS amplitudes, starting with the quarks. We varied the factorization scale, μ^2 , from Q^2 , used above, to $Q^2/2$ and $2Q^2$ for both sets and found the following variations, where the two sets agree fairly well with one another. At small ζ , we found a small variation at the input scale of 2 – 30% which reduces to about 2 – 10% at large Q^2 (we use $Q^2 = 100 \text{ GeV}^2$ throughout, as before) for both real and imaginary parts of both quark singlet and gluon. At large ζ , we find variations around 10 – 20% for both parts of the amplitude and for both quark and gluon at the input scale and at large Q^2 . In summary one can say that the scale dependence is not troublesome and that the uncertainties due to the chosen GPD are still much larger than those due to the factorization scale uncertainties.

B. The polarized case

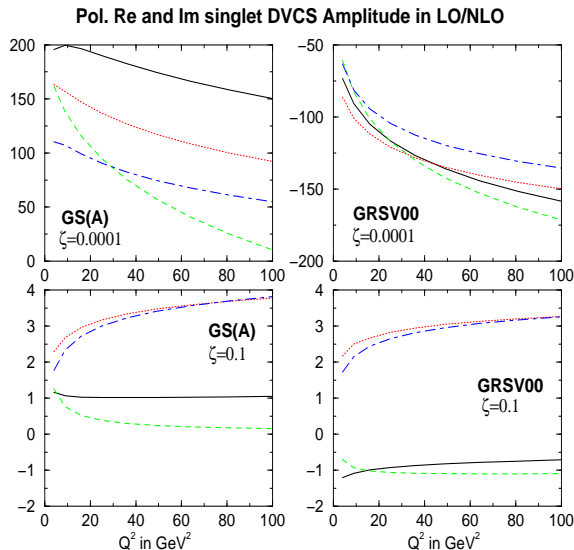


FIG. 7. Real and imaginary parts of the polarized quark singlet DVCS amplitude, as a function of Q^2 , for fixed ζ . The solid (dashed) curve is the real part in LO (NLO) and the dotted (dashed-dotted) curve is the imaginary part in LO (NLO).

For the polarized case we proceed exactly as we did for the unpolarized case starting in Fig. (7) with the absolute values of the real and imaginary parts of the polarized quark singlet amplitudes as functions of Q^2 . One immediately notices the very large NLO corrections

for the GS(A) input, whereas for the GRSV00 input the corrections are moderate to small, but typically around 10 – 15%. The very large corrections can be easily explained since in [14] it was shown that the GPD evolution drastically alters the shape of the GS(A) distribution in fact inverting its shape, whereas the shape of GRSV00 was almost unchanged and the absolute value changed only moderately. The difference in shape at small ζ was due to radically different assumptions about the polarized sea distributions: GRSV00 assume a flavor non-symmetric sea in contrast to the flavor-symmetric sea assumed by GS(A). At large ζ , where the shapes of the two input sets are similar we find that the shapes of the amplitudes in Q^2 are also very similar, whereas their absolute values differ. The relative changes in moving to NLO are very small for the imaginary parts whereas for the real parts, which are more sensitive to the sea, we find relatively large corrections for GS(A) and very moderate to small corrections 5 – 20% for GRSV00. One conclusion is that the NLO effects are very sensitive to shapes, which allows one to hope that small NLO corrections signal a correct shape for the GPDs. Note that at large ζ we find a stronger Q^2 dependence of the imaginary part relative to the unpolarized case, although for large Q^2 it still basically scales, whereas the real part shows a weaker Q^2 dependence, especially for GRSV00.

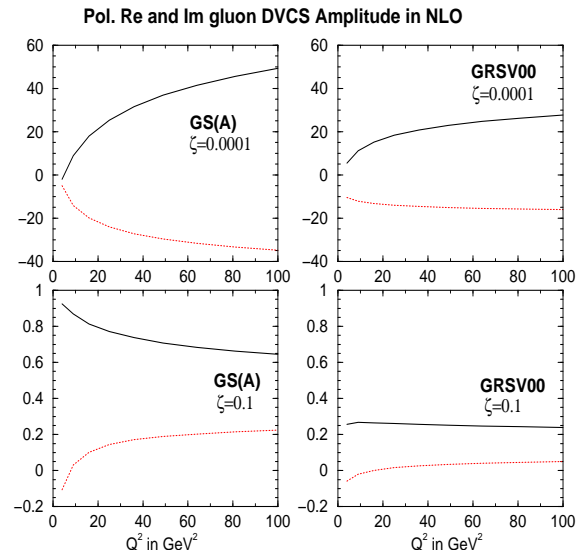


FIG. 8. The real and imaginary parts of the polarized gluon DVCS amplitude, as a function of Q^2 , for fixed ζ . The solid curves show the real part and the dotted curves show the imaginary part of the gluon amplitude.

Turning to the gluon in Fig. (8) we find it to be quite similar in shape and size for the two input sets, signaling a similarity in shape of the two input distributions. Note that the real part of the amplitude is positive for small and large ζ , exactly the opposite to the unpolarized case. The imaginary part of the amplitude is negative at small

ζ and only turns positive for larger Q^2 , again opposite to the unpolarized case. This behavior is due to the particular shape of the polarized gluon GPD at small and large ζ (see [14]).

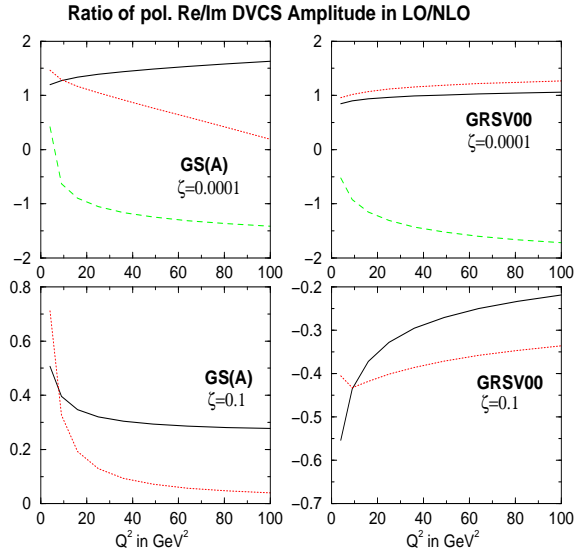


FIG. 9. The ratio of real to imaginary parts of the polarized quark singlet and gluon DVCS amplitudes, as a function of Q^2 , at fixed ζ . The solid (dotted) curves show the ratio for the quark singlet in LO (NLO) and the dashed curves show the ratio for the gluon in NLO.

In Fig.(9) we show the ratio of real to imaginary parts as a function of Q^2 , for fixed ζ . At small ζ , one immediately observes a strong deviation of the NLO ratio from the LO one, for the quarks of the GS(A) input set. This is not too surprising, given the observations made above. At large ζ , we again observe a flattening at large Q^2 as in the unpolarized case: the GS(A) result is flatter than the GRSV00 case where we still observe strong variations in Q^2 . For large Q^2 , the gluon ratio is very similar for both sets and fairly flat in Q^2 , although not as flat as in the unpolarized case. We did not plot the gluon ratio at large ζ since it has a very large value near the point where the imaginary part changes sign and thus would have completely swamped the quark result which we find more interesting here. Note that our LO ratio for the GS(A) model is in agreement with the values obtained by [17].

In Fig. (10) we plot the ζ -behaviour at fixed Q^2 and find a single power-like behaviour only for very small ζ (up to about 3×10^{-3}). Performing the same type of fits as in the unpolarized case, i.e. a simple two and four parameter fits, reveals a λ_0 between -0.4 to -0.55 , and a similar story for the four parameter fits. However, the second power, a_2 , is now substantially larger than in the unpolarized case, in order to be able to describe the large ζ behavior. The four parameter fit is able to describe the behavior of the amplitudes on the few percent

level. Thus the simple single-power Regge-type behavior observed in the unpolarized case is only valid at small ζ in the polarized case. This is because the polarized sea dies out even more quickly with increasing ζ , than the unpolarized one: therefore the highly asymmetric configurations necessary to produce a universal behavior in ζ become very rare. At large ζ they are almost completely gone.

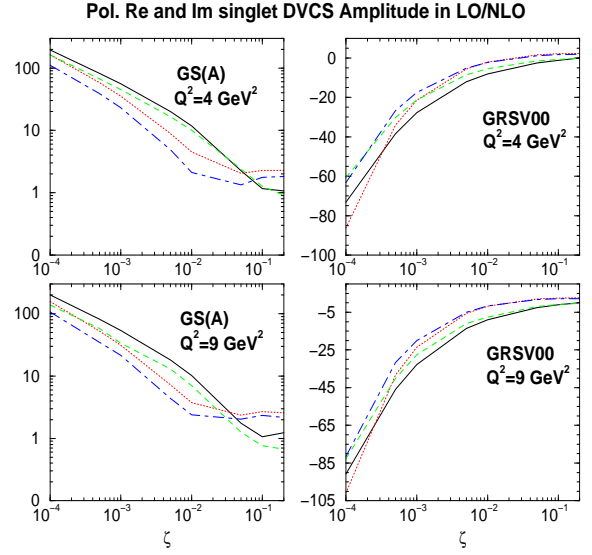


FIG. 10. Polarized real and imaginary parts of the quark singlet DVCS amplitude, as a function of ζ , for fixed Q^2 . The solid (dashed) curve is the real part in LO (NLO) and the dotted (dashed-dotted) curve is the imaginary part in LO (NLO).

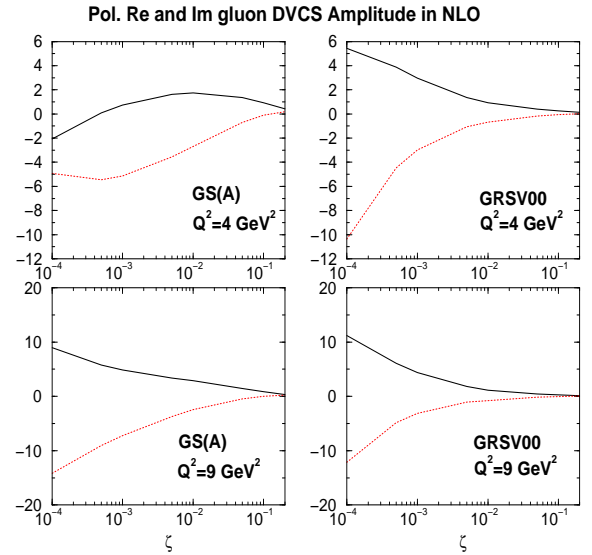


FIG. 11. Real and imaginary parts of the polarized gluon DVCS amplitude, as a function of ζ , at fixed Q^2 . The solid curve is the real part in NLO and the dotted curve is the imaginary part.

Turning to the gluon in Fig. (11) we illustrate that the behavior in ζ at an evolved scale is very similar in shape and size for the two input sets, despite the fact that they start off very different at the input scale. The evolution forces the distributions to be quite similar very quickly. The imaginary part is usually negative whereas the real part is usually positive.

The ζ -dependence of the ratio of real to imaginary parts, plotted in Fig. (12), is rather different to the unpolarized case, with a strong fluctuation in the gluon due to a sign change of one of the amplitudes around the spike (we sample at a finite number of points in ζ). The real part is typically much larger than the imaginary part, in contrast to the unpolarized case.

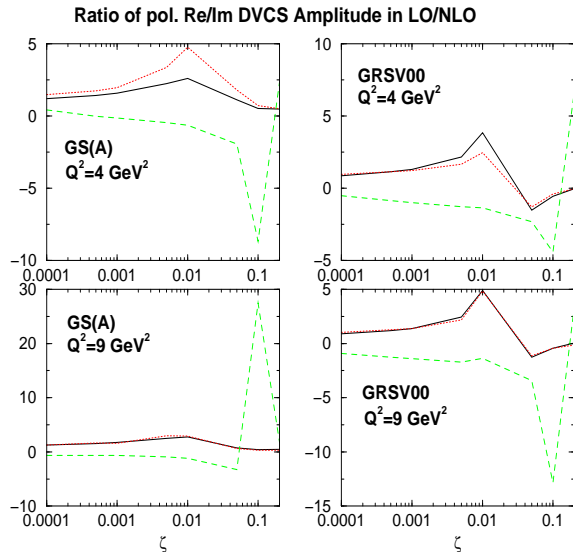


FIG. 12. The ratio of real to imaginary parts of the polarized quark singlet and gluon DVCS amplitudes, as a function of ζ at fixed Q^2 . The solid (dotted) curve is the ratio in LO (NLO) and the dashed curve is the ratio for the gluon, which starts at NLO.

Concerning the issue of the importance of the ERBL region, we find a similar picture to the unpolarized case, although the relative percentage contribution is smaller by about a factor of two, for both quarks and gluons. The influence of the subtraction term on the value of the real part of the amplitude is considerably less than in the unpolarized case, thus the ERBL region is weighed more heavily in the final value of the amplitude. This is in line with our observation of the deviations of the amplitudes from a single power in ζ , for relatively small values of ζ , compared to the unpolarized case (for which the ERBL region was of less importance as compared to the subtraction term).

Finally, we comment briefly on the scale dependence of the polarized amplitudes. We proceed in an identical manner to the unpolarized case in varying μ^2 . For small ζ , we find a similar variation with μ^2 as compared

to the unpolarized case for the quark singlet and larger variations for the gluon between 25 – 100% at the input scale and 10 – 50% at large Q^2 . At large ζ , we find, in line with the results of [18], variations in the real part of the quark singlet of around 50% at the input scale and around 25% at large Q^2 . The imaginary part only varies between 0 – 10% at the input scale and large Q^2 respectively, again in line with [18]. The gluon at large ζ is very well behaved and varies only between 10 – 20% for both real and imaginary parts at both the input scale and at large Q^2 . It is encouraging that the variations due to factorization scale changes can be safely neglected since the polarized distributions are even less well known than the unpolarized ones.

IV. GENERAL COMMENTS ON NLO AND NNLO CORRECTIONS

In this section we make some general comments about the structure of NLO corrections and expected NNLO corrections.

In [14] we pointed out that the relative shape change in the NLO evolution of GPDs, compared with LO, is due to a new class of integrable divergences, $\ln(1 - X/\zeta)^n / (1 - X/\zeta)^i$, $n, i = 0, 1, 2$, appearing in the region around ζ . The same type of integrable divergence also appears in the NLO coefficient functions, but is absent at LO, although one has an integrable singularity of the $1/(1 - X/\zeta)$ type. This fact alone helps to explain why one finds, in certain regions, large changes in going from LO to NLO in the amplitudes.

For DVCS observables the appearance of the gluon at NLO also changes things dramatically since the gluon contribution turns out to be of the same order as the quarks, at least at small ζ due to an extra factor of $1/\zeta$ in eq. (6). So, not only is a new quantity introduced, but one of the same order of magnitude as our LO quantities. Furthermore, with the unpolarized real part of the gluon amplitude being *negative* and of comparable size at small ζ as the real part of the quark amplitudes, observables sensitive to the real part, such as the azimuthal angle asymmetry are expected to change dramatically in NLO (see [15]). Conversely, the effect should not be as dramatic for observables sensitive to the imaginary part, since the NLO corrections are not as big and are *positive*, rather than negative (see [15]).

What would one expect in NNLO? From experience obtained in calculating forward coefficient functions, and some evolution kernels at $\mathcal{O}(\alpha_s^2)$, one would expect to see only the same type of integrable divergences reappearing, maybe with different powers in logs and rational functions, but not a new class of divergences which could radically alter the behavior of the amplitudes. Also, in contrast to moving from LO to NLO which gives the first gluon contributions, no new parton species appear at

NNLO. This leads us to speculate that the NNLO order corrections should be mild.

V. CONCLUSIONS

We have presented a detailed analysis of the quark singlet and gluon contributions to the polarized and unpolarized DVCS amplitudes at NLO, using NLO-evolved generalised partons distributions (GPDs) built from sensible input models. We have compared throughout with the LO results using the same input GPDs, and have therefore quantized the effect of the NLO corrections. These results are directly relevant to measurable quantities in $ep \rightarrow ep\gamma$ processes at the HERA and HERMES experiments, and hence may be used to constrain the GPDs at NLO. The most striking feature of our results is that for a given Q^2 the unpolarized amplitudes appear to exhibit a simple single-power behaviour in the skewedness parameter, ζ , over a very large range, apparently indicating a universal behaviour.

ACKNOWLEDGEMENTS

A. F. was supported by the DFG under contract # FR 1524/1-1. M. M. was supported by PPARC.

VI. APPENDIX

A. LO and NLO coefficient functions

The coefficient functions in eq. (6) are expanded in powers of α_s and read in general

$$\begin{aligned}
T^{q,V/A}(z) &= T^{q,LO}(z) + \frac{\alpha_s(\mu^2)}{2\pi} T^{q,V/A,,NLO}(z, Q^2/\mu^2) + \\
&\quad \mathcal{O}(\alpha_s^2) \mp (z \rightarrow -z), \\
T^{g,V/A}(z) &= T^{g,LO}(z) + \frac{\alpha_s(\mu^2)}{2\pi} T^{g,V/A,,NLO}(z, Q^2/\mu^2) + \\
&\quad \mathcal{O}(\alpha_s^2) \pm (z \rightarrow -z), \tag{11}
\end{aligned}$$

with $z = 2X/\zeta - 1$ where the upper (lower) sign refers to the unpolarized (polarized) case.

The LO and NLO coefficient functions for the right hand side of eq. (11) were taken from [18] and read:

$$\begin{aligned}
T^{q,LO}(z) &= \frac{1}{1-z}, \\
T^{g,LO}(z) &= 0,
\end{aligned}$$

$$\begin{aligned}
T^{q,NLO,V}(z) &= T^{q,NLO,A}(z) - \frac{C_F}{1+z} \ln \frac{1-z}{2}, \\
T^{q,NLO,A}(z) &= \frac{C_F}{2(1-z)} \left[\left(2 \ln \frac{1-z}{2} + 3 \right) \times \right. \\
&\quad \left. \left(\ln \frac{Q^2}{\mu^2} + \frac{1}{2} \ln \frac{1-z}{2} - \frac{3}{4} \right) - \frac{27}{4} - \frac{1-z}{1+z} \ln \frac{1-z}{2} \right], \\
T^{q,NLO,V}(z) &= -T^{g,NLO,A}(z) + \\
\frac{N_F}{2} &\left[\frac{1}{1-z} \left(\ln \frac{Q^2}{\mu^2} + \ln \frac{1-z}{2} - 2 \right) + \frac{\ln \frac{1-z}{2}}{1+z} \right], \\
T^{q,NLO,V}(z) &= \frac{N_F}{2} \left[\left(\frac{1}{1-z^2} + \frac{\ln \frac{1-z}{2}}{(1+z)^2} \right) \times \right. \\
&\quad \left. \left(\ln \frac{Q^2}{\mu^2} + \ln \frac{1-z}{2} - 2 \right) - \frac{\ln^2 \frac{1-z}{2}}{2(1+z)^2} \right], \tag{12}
\end{aligned}$$

where the LO quark coefficient is normalized in such a way that, in the forward limit, after properly restoring the dependence on both skewedness parameters, one recovers the LO DIS coefficient $\delta(1-x)$ and the NLO gluon coefficient is normalized such that one recovers $\frac{1}{2}C_g^{DIS}$.

In the interval $[0, \zeta]$, the above coefficients are strictly real. However, in the interval $[\zeta, 1]$, they split into a real and imaginary parts, which can be easily deduced from eq. (12).

B. LO and NLO subtraction functions

In this section, we present the subtraction functions needed in our implementation of the Cauchy principal value prescription of eq.(7), i.e. the integrals

$$\begin{aligned}
I^q(\zeta) &= \zeta \int_0^1 dX \left[T^q \left(\frac{2X}{\zeta} - 1 \right) \mp T^q \left(1 - \frac{2X}{\zeta} \right) \right], \\
I^g(\zeta) &= \zeta \int_0^1 dX \left[T^g \left(\frac{2X}{\zeta} - 1 \right) \pm T^g \left(1 - \frac{2X}{\zeta} \right) \right], \tag{13}
\end{aligned}$$

with the upper and lower signs for the unpolarized and polarized cases, respectively. This generates real and imaginary parts for the subtraction functions, $I^{q,g}$, given below. One has to be careful to take the appropriate sheet of the Riemann surface for the logarithms in order to obtain the correct imaginary parts, i.e. to use the right $i\epsilon$ prescription consistently. In order to ensure the correctness of the results below, we cross checked them both with MATHEMATICA and MAPLE.

$$I^{q,LO}(\zeta) = \zeta \left[\frac{1}{2} i\pi - \frac{1}{2} \ln \left(\frac{1-\zeta}{\zeta} \right) \right], \tag{14}$$

$$\begin{aligned}
I^{q,NLO,A}(\zeta, Q^2, \mu^2) = & C_F \zeta \left[\frac{\pi^2}{24} + \right. \\
& \frac{1}{4} \ln \frac{Q^2}{\mu^2} \left(\pi^2 - 3 \ln \left(\frac{1-\zeta}{\zeta} \right) - \ln^2 \left(\frac{1-\zeta}{\zeta} \right) \right) - \\
& \frac{1}{4} \text{Li}_2 \left(1 - \frac{1}{\zeta} \right) + \frac{1}{4} \ln(\zeta) \ln(1-\zeta) + \\
& \frac{1}{4} (\pi^2 + 9) \ln \left(\frac{1-\zeta}{\zeta} \right) - \frac{1}{12} \ln^3 \left(\frac{1-\zeta}{\zeta} \right) + \\
& i\pi \left[\frac{\pi^2}{12} - \frac{9}{4} + \frac{1}{4} \ln(\zeta) - \frac{1}{4} \ln^2 \left(\frac{1-\zeta}{\zeta} \right) \right. \\
& \left. \left. - \ln \frac{Q^2}{\mu^2} \left(\frac{1}{2} \ln \left(\frac{1-\zeta}{\zeta} \right) - \frac{3}{4} \right) \right] \right], \quad (15)
\end{aligned}$$

$$\begin{aligned}
I^{q,NLO,V}(\zeta, Q^2, \mu^2) = & C_F \zeta \left[\frac{\pi^2}{8} + \right. \\
& \frac{1}{4} \ln \frac{Q^2}{\mu^2} \left(\pi^2 - 3 \ln \left(\frac{1-\zeta}{\zeta} \right) - \ln^2 \left(\frac{1-\zeta}{\zeta} \right) \right) - \\
& \frac{3}{4} \text{Li}_2 \left(1 - \frac{1}{\zeta} \right) + \frac{3}{4} \ln(\zeta) \ln(1-\zeta) + \\
& \frac{1}{4} (\pi^2 + 9) \ln \left(\frac{1-\zeta}{\zeta} \right) - \frac{1}{12} \ln^3 \left(\frac{1-\zeta}{\zeta} \right) + \\
& i\pi \left[\frac{\pi^2}{12} - \frac{9}{4} + \frac{3}{4} \ln(\zeta) - \frac{1}{4} \ln^2 \left(\frac{1-\zeta}{\zeta} \right) \right. \\
& \left. \left. - \ln \frac{Q^2}{\mu^2} \left(\frac{1}{2} \ln \left(\frac{1-\zeta}{\zeta} \right) - \frac{3}{4} \right) \right] \right], \quad (16)
\end{aligned}$$

$$\begin{aligned}
I^{g,NLO,A}(\zeta, Q^2, \mu^2) = & N_F \zeta \left[\frac{1}{4} + \right. \\
& \frac{\pi^2}{16} \zeta - \frac{1}{8} \ln \frac{Q^2}{\mu^2} \left(1 + \zeta \ln \left(\frac{1-\zeta}{\zeta} \right) \right) + \\
& \frac{\zeta}{4} \ln \left(\frac{1-\zeta}{\zeta} \right) - \frac{\zeta}{16} \ln^2 \left(\frac{1-\zeta}{\zeta} \right) + \\
& \left. i\pi \zeta \left[2 - \ln \frac{Q^2}{\mu^2} - \ln \left(\frac{1-\zeta}{\zeta} \right) \right] \right], \quad (17)
\end{aligned}$$

$$\begin{aligned}
I^{g,NLO,V}(\zeta, Q^2, \mu^2) = & N_F \zeta \left[-\frac{1}{4} + \right. \\
& \frac{\pi^2}{16} \left(\frac{3}{4} - \zeta \right) + \frac{1}{8} \ln \frac{Q^2}{\mu^2} \left(1 - (2-\zeta) \ln \left(\frac{1-\zeta}{\zeta} \right) \right) + \\
& \frac{2-\zeta}{4} \ln \left(\frac{1-\zeta}{\zeta} \right) + \frac{2-\zeta}{16} \ln^2 \left(\frac{1-\zeta}{\zeta} \right) + \\
& \frac{1}{4} \text{Li}_2 \left(1 - \frac{1}{\zeta} \right) - \frac{1}{4} \ln(\zeta) \ln(1-\zeta) + \\
& \left. i\pi \left[(2-\zeta) \left(2 - \ln \frac{Q^2}{\mu^2} - \ln \left(\frac{1-\zeta}{\zeta} \right) \right) - 2 \ln(\zeta) \right] \right]. \quad (18)
\end{aligned}$$

-
- [1] D. Müller *et al.*, Fortsch. Phys. 42 (1994) 101.
 - [2] A. V. Radyushkin, Phys. Rev. D 56 (1997) 5524.
 - [3] X. Ji, J. Phys. G 24 (1998) 1181.
 - [4] M. Diehl *et al.*, Phys. Lett. B 411 (1997) 193.
 - [5] M. Vanderhaeghen, P. A. M. Guichon and M. Guidal, Phys. Rev. D 60 (1999) 094017.
 - [6] J. C. Collins and A. Freund, Phys. Rev. D 59 (1999) 074009.
 - [7] L. Frankfurt, A. Freund and M. Strikman, Phys. Rev. D 58 (1998) 114001; Erratum-ibid. D59 (1999) 119901 and Phys. Lett. B 460 (1999) 417, A. Freund and M. Strikman, Phys. Rev. D 60 (1999) 071501.
 - [8] The HERMES Collab., hep-ex/0106068; P.R. Saull, for ZEUS Collab., hep-ex/0003030; L. Favart, for H1 and ZEUS Collabs., hep-ex/0106067; J. P. Chen, for Jefferson Lab, <http://www.jlab.org/~sabatie/dvcs/index.html>.
 - [9] A. V. Belitsky *et al.*, Phys. Lett. B 437 (1998) 160; A. V. Belitsky, A. Freund and D. Müller, Nucl. Phys. B574 (2000) 347.
 - [10] V. Yu. Petrov *et al.*, Phys. Rev. D 57 (1998) 4325.
 - [11] L. Frankfurt *et al.*, Phys. Lett. B 418 (1998) 345, Erratum-ibid. B429 (1998) 414; A. Freund and V. Guzey, Phys. Lett. B 462 (1999) 178.
 - [12] V. N. Gribov and L. N. Lipatov, Sov. J. Phys 15 (1972) 438, 675; Yu. L. Dokshitzer, Sov. Phys. JETP 46 (1977) 641; G. Altarelli. and G. Parisi, Nucl Phys B126 (1977) 298.
 - [13] A. V. Efremov and A. V. Radyushkin, Theor. math. Phys. 42 (1980) 97, Phys Lett. B94 (1980) 245; S. J. Brodsky and G. P. Lepage, Phys Lett. B87 (1979) 359; Phys. Rev. D22 (1980) 2157.
 - [14] A. Freund and M. McDermott, hep-ph/0106115.
 - [15] A. Freund and M. McDermott, hep-ph/0106124.
 - [16] A. V. Belitsky *et al.*, hep-ph/0103343.
 - [17] A. V. Belitsky *et al.*, Nucl. Phys. B 593 (2001) 289.
 - [18] A. V. Belitsky *et al.*, Phys. Lett. B 474 (2000) 163.
 - [19] K. Golec-Biernat and A. D. Martin, Phys. Rev. D 59 (1999) 014029.
 - [20] A. V. Radyushkin, Phys. Rev. D59 (1999) 014030.
 - [21] N. Kivel, M. V. Polyakov and M. Vanderhaeghen, Phys. Rev. D 63 (2001) 114014.
 - [22] M. V. Polyakov and C. Weiss, Phys. Rev. D 60 (1999) 114017.
 - [23] M. Glück, E. Reya and A. Vogt, Eur. Phys. J. C 5 (1998) 461; M. Glück *et al.*, Phys.Rev. D63 (2001) 094005; We evolve from the low input scales up to $Q_0 = 2$ GeV, using conventional (forward) DGLAP evolution.
 - [24] A. D. Martin, R. G. Roberts and W. J. Stirling, Phys. Lett. B 354 (1995) 155; T. Gehrmann, W. J. Stirling, Phys. Rev. D 53 (1996) 6100.
 - [25] A. Freund and M. McDermott, "A detailed analysis of DVCS at next-to-leading order", preprint in preparation.
 - [26] L. Frankfurt, M. McDermott and M. Strikman, JHEP 0103 (2001) 045.